Atmospheric Response to a Partial Solar Eclipse over a Cotton Field in Central California

MATTHIAS MAUDER AND R. L. DESJARDINS
Research Branch, Agriculture and Agri-Food Canada, Ottawa, Ontario, Canada

STEVEN P. ONCLEY
National Center for Atmospheric Research, Boulder, Colorado*

IAN MACPHERSON
Flight Research Laboratory, Institute for Aerospace Research, National Research Council, Ottawa, Ontario, Canada

(Manuscript received 15 May 2006, in final form 5 February 2007)

ABSTRACT

The partial solar eclipse on 11 July 1991 in central California, with 58.3% maximum coverage, provided an exceptional opportunity to study the temporal response of processes in the atmospheric boundary layer to an abrupt change in solar radiation. Almost laboratory-like conditions were met over a cotton field, since no clouds disturbed the course of the eclipse. Tower-based and complementing aircraft-based systems monitored the micrometeorological conditions over the site. Temperature profile measurements indicated neutral stratification during the maximum eclipse in contrast to the unstable conditions before and after the eclipse. Accordingly, the sensible heat exchange completely stopped, as a wavelet analysis of the tower measurements and airborne eddy-covariance measurements showed. Turbulent fluxes of water vapor, carbon dioxide, and ozone were reduced by approximately ⅔ at the peak of the eclipse. Wavelet analysis further indicated that the same eddies contributed to the turbulent transport of water vapor and carbon dioxide, whereas sensible heat was transported by different ones. An analysis of the decay of turbulent kinetic energy followed a power law of time with an exponent of −1.25. The response of the sensible heat flux was 8–13 min delayed relative to the solar forcing, whereas no significant time lag could be detected for the turbulent fluxes of air constituents.

1. Introduction

A solar eclipse causes a distinct change in the solar radiation—the forcing for many processes in the atmospheric boundary layer. This change is more abrupt than during the usual shift from day to night at either sunrise or sunset. When a solar eclipse occurs around midday during a time of strong convective boundary layer development, an ecosystem experiences a sudden drop in solar radiation and shortly afterward a sudden turn-on. Therefore, a solar eclipse during clear-sky conditions provides an extraordinary opportunity to study the response of the boundary layer under such conditions, and to characterize different turbulent fluxes. This is an extreme case that might help with the understanding of more common occurrences like transitions in the early evening or during cloud passages.

Several scientists have reported measurements obtained during past solar eclipses. Anderson (1999) gives an overview of meteorological changes in the entire atmosphere during a total solar eclipse. He describes a stabilization of the thermal stratification in the surface layer with a surface-based inversion and a reduction in turbulent transport. According to his information, this reaction usually happens with a few minutes delay to the actual totality.

The surface energy budget measurements of Stewart and Rouse (1974) for an arctic site near the Hudson Bay coast in Canada showed a significant drop of the sensible and the latent heat flux to zero. At the same

* The National Center for Atmospheric Research is sponsored by the National Science Foundation.

Corresponding author address: Matthias Mauder, Research Branch, Agriculture and Agri-Food Canada, 960 Carling Ave., Ottawa, ON K1A0C6, Canada.
E-mail: MauderM@agr.gc.ca

DOI: 10.1175/2007JAMC1495.1

time, the air temperature fell 10°C during that eclipse on 10 July 1972, which reached 90% totality. Similarly, over a desert site in New Mexico, an 88% reduction of the solar radiation led to sensible heat fluxes going down to zero and neutral stratification in absence of a significant latent heat flux during the eclipse of 10 May 1994 (Eaton et al. 1997). Also the variances of all wind components and the resulting turbulent kinetic energy were significantly reduced.

The study of Foken et al. (2001) addresses in particular the temporal delay of the atmospheric and ecosystem response to radiative forcing. Their measurements were conducted over a corn field in southern Germany during a total eclipse on 11 August 1999. Although those observations were disturbed by a thin cover of stratocumulus clouds, Foken et al. (2001) were able to determine the time lag between the peak of the eclipse and the minimum of several atmospheric parameters such as friction velocity, sensible heat flux, latent heat flux, carbon dioxide flux, and ozone flux based on 5-min covariances. Most of the minima of the turbulent fluxes almost coincided with the totality, except the latent heat flux and the friction velocity, which reached a minimum 25 min later. A wavelet analysis was performed on net radiation, air temperature, and wind velocity in order to investigate the temporal scales of the highly nonstationary processes during the eclipse.

Anfossi et al. (2004) analyzed measurements over grassland in northern France for the same eclipse. In that case, variances of the three wind components and turbulent kinetic energy showed a minimum 40 min after the totality. That study analyzes the decay of convective turbulence during the eclipse in comparison with a theoretical model by Goulart et al. (2003). Decay of convective turbulence occurs usually during the evening transition in the residual layer above the stable boundary layer, which develops over the cooling ground. That process is difficult to measure under regular conditions, and an eclipse provides an extreme situation to validate such models. That issue is also addressed by large-eddy simulation (LES) studies about a convective boundary layer, in which the surface heat flux is set to zero suddenly (Nieuwstadt and Brost 1986) or gradually (Sorbjan 1997).

Similar to previous meteorological studies on solar eclipses, our study aims to investigate the atmospheric response to that rapid change in solar forcing. It focuses on the processes in the atmospheric boundary layer over the measurement site—a cotton field in central California. This eclipse was partial and occurred in the late morning shortly before noon, while air temperatures and turbulence activity are usually increasing. A sudden drop in solar forcing under such conditions will cause a highly nonstationary response in turbulent transport, which provides a challenge for the methodology to analyze the data.

To address this problem, a wavelet transform is applied. For the sensible heat flux, results of such a wavelet transform were already presented by Schayes et al. (2002) for the eclipse on 11 August 1999. We investigate the turbulent fluxes of sensible heat, water vapor, carbon dioxide, and ozone. Measurements from ground-based and airborne systems are analyzed. The wavelet methodology is used in order to obtain quantitative results for turbulent fluxes at a sufficiently high temporal resolution on the order of 1 min without neglecting flux contributions from frequencies lower than this averaging time, which is impossible with the traditional eddy-covariance technique. This wavelet analysis allows studying the scales of turbulent fluxes and how they evolve during the course of the eclipse. It makes it possible to investigate how flux scales react to the decrease and sudden increase of solar radiation, and it helps to better understand some transition conditions in the surface layer.

2. Site and measurements

The measurements for this study about the influence of an eclipse on the boundary layer structure were conducted over a cotton field near Fresno in the San Joaquin Valley of California (36°48′50″N, 120°40′38″W, 74 m MSL) on 11 July 1991. The eclipse started at 1012 Pacific daylight time (PDT) (first contact). The maximum coverage of 58.3% was reached at 1123 PDT. The sun's disk was completely uncovered by the moon's again at 1238 PDT (fourth contact).

The measurements were conducted as part of the California Ozone Deposition Experiment (CODE) (Pederson et al. 1995). The complete instrumentation at the cotton site was operated by the National Center for Atmospheric Research (NCAR). All data were collected using their Atmosphere–Surface Turbulent Exchange Research (ASTER) facility (Businger et al. 1990). One momentum/heat flux tower, one scalar flux tower for water vapor and CO_2, one psychrometer profile tower, and one wind profile tower were deployed. All ASTER fluxes presented in this study were measured at 5 m above ground level. The sensible heat flux was measured by a University of Washington (UW) sonic anemometer (Zhang et al. 1986) with a sampling rate of 20 Hz. A combination of a UW sonic and a Campbell KH20 krypton hygrometer was used for the latent heat flux measurement. A prototype CO_2 sensor by Kohsiek (1991) was also used for this study. It was found to drift and have a temperature sensitivity (Oncley et al. 1993), so empirical corrections were ap-

plied based on field calibrations done six days later. Significant biases may still have been present in these corrected data. However, the gain (and thus the fluxes) should be accurate to at least 20% based on a comparison with a simultaneously deployed slow response sensor. The profile tower was equipped with five psychrometers recorded at 1 Hz. A pair of Eppley Precision Spectral Pyranometers and two Eppley Precision Infrared Radiometers was deployed to measure shortwave and longwave radiation in both directions, also at a sampling rate of 1 Hz.

During the solar eclipse, the Twin Otter research aircraft of the Canadian National Research Council (NRC) flew over this site (MacPherson 1992). The results of the aircraft measurements during CODE are summarized in MacPherson et al. (1995). During this field campaign, the Twin Otter was equipped with a Rosemount 858 five-hole probe to measure wind speed at 16 Hz. Air temperature was measured by a Rosemount fast-response 102DJ1CG probe mounted on the port side of the nose. Water vapor and carbon dioxide were measured using an ESRI infrared gas analyzer (Brach et al. 1981) with a frequency response of 10 Hz. A prototype analyzer on lease from the Institute of Atmospheric Physics at DLR (German Aerospace Research facility), which had a frequency response of at least 10 Hz (Schmidt et al. 1991), reported the ozone data. Incident shortwave radiation was measured with a Kipp and Zonen CM-11.

The airborne measurements of the NRC Twin Otter on 11 July 1991 started at 1013 PDT, shortly after the first contact of the moon's disk, and ended at 1216 PDT, shortly before the end of the eclipse. During this period, the aircraft flew a northwest–southeast track and an east–west track each 16 times. These two tracks intersected close to the position of the towers on the cotton site (Fig. 1). Irrigated cotton was the dominant canopy type below the flight tracks. Other crops in the study area were melons, tomatoes and beans, which were also at a fully green stage. The flight level of the airplane was approximately 30 m above terrain. Each track averaged 6.3 km long, which corresponds to a duration of 105 s at a groundspeed of 60 m s^{-1}. Desjardins et al. (1995) show that measurements from the Twin Otter aircraft and the ground-based tower measurements lead to estimates of turbulent fluxes that were within 10% of each other.

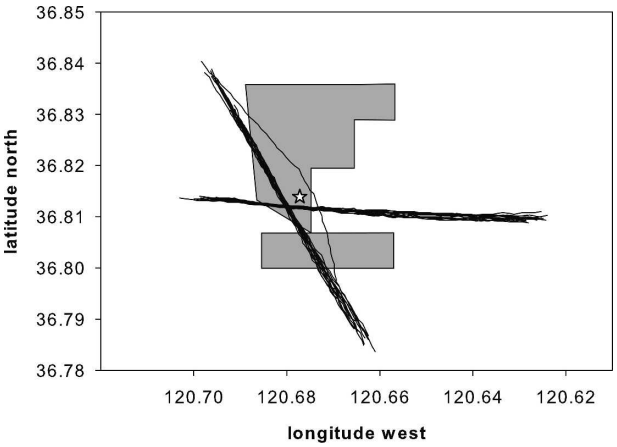

FIG. 1. Flight tracks of the NRC Twin Otter research aircraft during the eclipse between 1013 and 1216 PDT 11 Jul 1991; the location of the cotton site is indicated by a star; the area covered with cotton plants is highlighted in gray.

3. Data processing

a. Eddy-covariance technique

Turbulent fluxes from the aircraft measurements were calculated for each track using the eddy-covariance technique (Swinbank 1951). The delay between displaced sensors was corrected using a cross-correlation analysis (Chahuneau et al. 1989). A detailed description of the Twin Otter flux calculations is provided in MacPherson (1990). No detrending or filtering was applied in this case to avoid possible low-frequency spectral losses through the averaging procedure as described by Finnigan et al. (2003).

b. Ogive analysis

Since the changes in solar forcing during an eclipse generally happen on the scale of a few minutes, the potential response in atmospheric turbulence should be analyzed on the same time scale. Therefore, it is interesting to study variances and covariances on the scale of 1 or 2 min, especially to determine the time delay of the atmospheric response. An ogive analysis (Desjardins et al. 1989; Friehe 1991; Oncley et al. 1996) helps to determine which averaging time would be sufficiently long for the calculation of eddy-covariance calculations. An ogive Og represents the cumulative integral over a cospectrum Co starting from the highest frequency f,

$$\mathrm{Og}(f_0) = \int_{\infty}^{f_0} \mathrm{Co}(f)\, df. \tag{1}$$

Such an analysis was conducted for data from the ASTER flux tower (Fig. 2a) and for data from the Twin Otter aircraft (Fig. 2b). A Fourier transform was applied to compute the cospectra.

An ogive function should reach a plateau value to justify the assumption that the whole cospectrum of flux contributions is covered for a certain averaging period. For the ASTER site, most of the flux contribu-

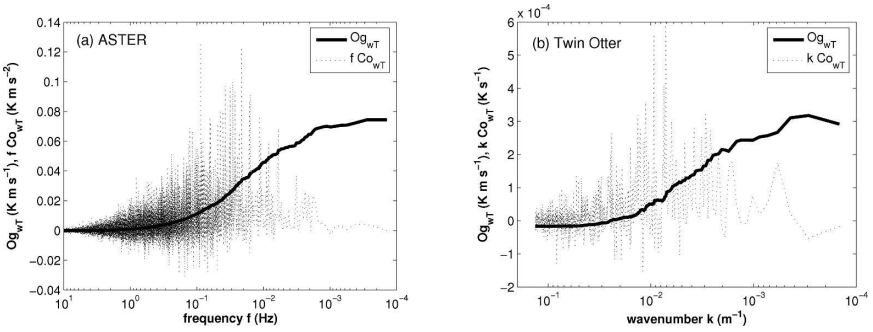

FIG. 2. Ogive and Fourier cospectrum between vertical wind velocity w and temperature T in area-preserving semilogarithmic presentation: (a) ASTER data from 1200 to 1400 PDT 11 Jul 1991; (b) Twin Otter data from the flight track between 1210 and 1212 PDT 11 Jul 1991.

tions have frequencies between 10^{-1} and 10^{-3} Hz, where the ogive (Fig. 2a) has its steepest slope. However, the cumulative flux is still slightly increasing even for frequencies lower than 1.1×10^{-3} Hz, which is equivalent to a period of 15 min. This means an eddy-covariance calculation with 15-min averaging time does not cover the full cospectrum of flux contributions. It underestimates the turbulent flux by at least 10%, since the ogive value for the 120-min period (1.4×10^{-4} Hz) is 10% higher than the value for the 15-min period. However, for investigating the atmospheric response on the solar eclipse, periods smaller than 15 min are desirable.

Looking at the Twin Otter aircraft measurements between 1210 and 1212 PDT (Fig. 2b), most of the turbulent flux is carried out in eddies of wavenumbers between 10^{-2} and 4×10^{-4} m^{-1}. For lower wavenumbers, the cumulative flux is slightly decreasing again. The ogives of other flight tracks were similar. Therefore, we assume that the entire cospectrum of flux contributions is captured when we calculate the covariance over one flight track.

c. Wavelet analysis

The wavelet transform can be used to analyze time series that contain nonstationary power at many different frequencies (Daubechies 1990). It does not require stationarity as the eddy-covariance method, which is based on Reynolds averaging (e.g., Terradellas et al. 2001; Cuxart et al. 2002; Strunin and Hiyama 2004). The wavelet analysis transforms a time series into a time-scale space, whereas the traditional Fourier analysis is a transformation into the spectral domain.

The wavelet software that was used for this study is based on the code provided by C. Torrence and G. Compo (available online at http://paos.colorado.edu/research/wavelets/). In general, a continuous wavelet transform of a discrete sequence $x(n)$ is defined as convolution of $x(n)$ with a wavelet function,

$$W_x(a, b) = \sum_{n=0}^{N} x(n)\psi^*_{p,a,b}(n), \tag{2}$$

where $W_x(a, b)$ are called the wavelet coefficients as a function of scale or dilatation parameter a and shift or translation parameter b; $\psi^*_{p,a,b}$ is the complex conjugate of a wavelet function. Different functions can serve as mother wavelet, for example, the Haar wavelet, the Mexican hat wavelet, or the Morlet wavelet. For this study the Morlet wavelet was selected, since it has been proven to be suitable for the analysis of atmospheric turbulence (e.g., Attié and Durand 2003; Strunin and Hiyama 2004; Terradellas et al. 2005; Thomas and Foken 2005).

The transformed wavelet coefficients can be squared to obtain the wavelet scalogram $|W_x(a, b)|^2$ (Kumar and Foufoula-Georgiou 1994). Averaging that matrix yields the wavelet spectrum (Hudgins et al. 1993),

$$E_x = \frac{\delta t}{C_\delta}\frac{1}{N}\sum_{n=0}^{N-1} |W_x(a, b)|^2, \tag{3}$$

where C_δ is a reconstruction factor, which has a constant value of 0.776 for this Morlet wavelet (Torrence and Compo 1998), and δt is the time step of the time series. The wavelet spectrum is analogous to a Fourier spectrum and should coincide with it. Consequently, the variance of the signal x can be calculated as sum over all scales,

$$\sigma_x^2 = \delta j \sum_{j=0}^{J} \frac{E_x(j)}{a(j)}, \tag{4}$$

where δj is nondimensional and determines the spacing between discrete scales of the wavelet transform. It

was chosen to be 0.25 for this analysis according to the recommendation of Torrence and Compo (1998).

Similarly, the wavelet cross-scalogram can be defined as $W_x(a, b)W_y^*(a, b)$, where $W_y^*(a, b)$ is the complex conjugate of a the wavelet transform of another signal $y(n)$. Averaging that matrix yields the wavelet cross-spectrum (Hudgins et al. 1993),

$$E_{xy} = \frac{\delta t}{C_\delta}\frac{1}{N}\sum_{n=0}^{N-1} W_x(a, b)W_y^*(a, b). \quad (5)$$

The cospectrum, which is often used in meteorology to study spectral contributions to turbulent fluxes, can then be calculated from the real part of the cross-spectrum (e.g., Stull 1988). The covariance of a signal x and another signal y can be calculated as

$$\mathrm{cov}_{xy} = \delta j \sum_{j=0}^{J} \frac{E_{xy}(j)}{a(j)}. \quad (6)$$

The averaging in the time domain [Eqs. (3) and (5)] does not necessarily have to be applied for the entire time period of the wavelet analysis. Averaging over shorter periods is also possible (Torrence and Compo 1998). This property of Eqs. (3) and (5) is of particular interest for the analysis of the highly nonstationary time series during the solar eclipse, since it allows the calculation of turbulent fluxes for short averaging times like 1 or 2 min without neglecting flux contributions from periods longer than the averaging time.

Consequently, the turbulent fluxes during the solar eclipse were calculated using modifications of Eqs. (5) and (6), in which E_{xy} was not averaged over all N, but over a shorter time period, in this case 1 min. In Eq. (6), cov_{xy} was not calculated as sum over the number of all scale steps J, but only for those j that were not within the cone of influence (COI), in which edge effects due to the finite length of a time series become important. The influence of edge effects is very strong at the beginning and at the end of a cross-scalogram. Only wavelet covariances are presented in this paper that sum up at least flux contributions of periods up to 15 min.

d. Flux conversions and corrections

After the calculation of the wavelet covariances, all necessary flux conversions and corrections were conducted using the software package TK2 developed by Mauder and Foken (2004). The coordinate system was rotated into the mean streamlines (Wilczak et al. 2001). Spectral loss in the high-frequency part was corrected (Moore 1986). The cross-sensitivity of the krypton hygrometer was corrected (Tanner et al. 1993). The sensible heat flux was calculated from sonic anemometer data using the conversion of Schotanus et al. (1983). Density effects due to heat and water vapor transfer were corrected according to Webb et al. (1980).

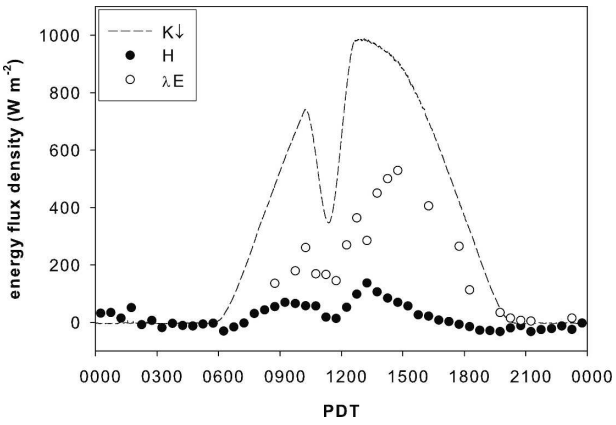

FIG. 3. Incoming shortwave radiation $K\downarrow$, sensible heat flux H, and latent heat flux λE on 11 Jul 1991, the day of the eclipse.

4. Results and discussion

a. Radiation, turbulent energy fluxes, and surface temperature

At the time of the peak of the eclipse, the incoming shortwave radiation over the cotton site was reduced by 60.5% compared to the value at the same time of the following day (Fig. 3). This is slightly more than the value for the maximum coverage of 58.3% from astronomical calculations. The 30-min eddy-covariance fluxes of sensible and latent heat showed a distinct negative deviation during the eclipse from their regular diurnal course (Fig. 3).

Surface temperatures had an overall positive trend on the day of the eclipse until 1330 PDT (Fig. 4). The reduced solar forcing during the eclipse caused a drop around the maximum coverage though. Two more drops occurred in the surface temperature curve, one of them around 1000 PDT, shortly before the beginning of the eclipse, and another one around 1310 PDT, shortly after the fourth contact.

b. Profiles of temperature and humidity

During the eclipse, the increase of air temperature in the developing convective boundary layer was brought to halt (Fig. 5). The reduction of solar radiation was sufficiently large that the thermal stratification became neutral but not stable. This can be seen in the temperature ASTER profile measurements (Fig. 5). The thermal stratification changed from unstable before the eclipse (1012 PDT) to almost neutral around 1123 PDT.

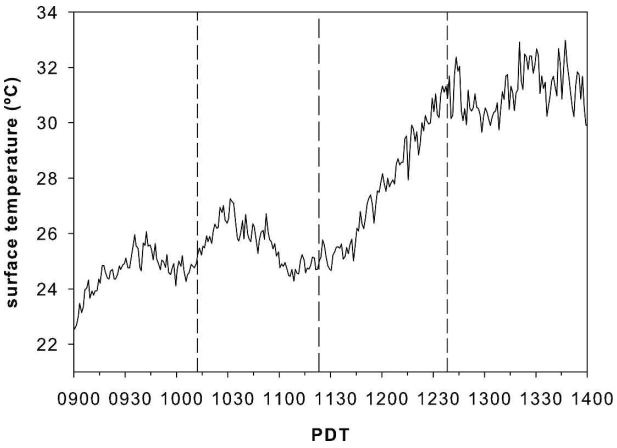

FIG. 4. Surface temperatures above the cotton canopy from the ASTER system; dashed vertical lines indicate the first contact (1012 PDT), the maximum of the eclipse (1123 PDT), and the last contact (1238 PDT).

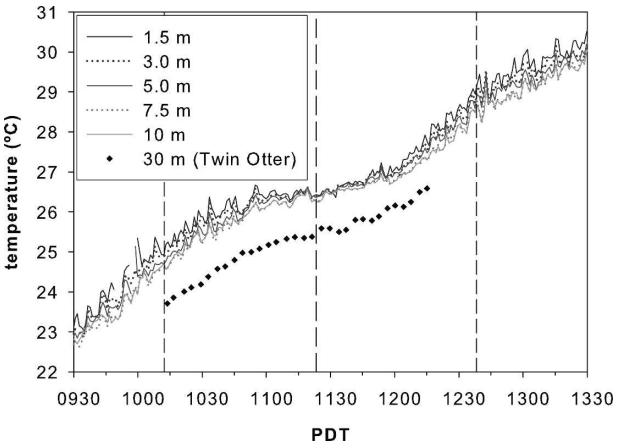

FIG. 5. Air temperatures from the ASTER system at five different levels above ground, plus the air temperature from the NRC Twin Otter aircraft at a level of 30 m; dashed vertical lines as in Fig. 4.

Neutral conditions persisted for almost 15 min and turned to unstable again afterward. A plateau in air temperature readings similar to the ASTER measurements was also found for the Twin Otter data during the eclipse. However, no surface-based inversion could be observed, which had been reported for a total eclipse by Anderson (1999).

The moisture profile measurements are shown in Fig. 6. The difference between the water vapor pressure at 1.5 and 10 m was around 2 hPa before and after the eclipse. The vertical moisture gradient, which is the driving force for the latent heat flux, became smaller during the eclipse but it was not zero. The difference between the 1.5- and the 10-m level decreased to approximately 1 hPa from 1120 to 1130 PDT. For most of the time before and after the maximum of the eclipse, the Twin Otter moisture measurements were similar to those at the 10-m tower level. Only the two runs directly after 1123 PDT showed significantly lower water vapor readings. It remains unclear whether this is an eclipse effect or not.

c. *Variances of wind speed and decay of turbulent kinetic energy*

During the eclipse, when the surface layer became less unstable, wind fluctuations became less intense. This can be seen in Fig. 7, which presents the 1-min wavelet variances of both the horizontal and the vertical wind speed. Both variances and therefore also the turbulent kinetic energy were reduced during the maximum coverage of the eclipse. This reduction was superimposed on a temporal trend of both variances between 0930 and 1330 PDT. Wind speed variances increased as a result of the development of the convective boundary layer, which was interrupted by the eclipse event on that day. The two drops in the horizontal wind speed variance at 1010 and 1320 PDT were possibly related to the two drops in surface temperature 10 min before. In the same way the increasing wind variances around 1040 PDT could be explained by a peak in surface temperatures at 1030 PDT (Fig. 4). Large wind fluctuations could be observed before 1045 and after 1215 PDT. In between, during the 90 min around the maximum coverage, wind speed variations returned to a lower level comparable to the situation earlier in the morning at around 0930 PDT. No such obvious explanation could be found for the wind speed variance drop with a minimum at 1235 PDT. However, the following analysis shows that it was related to the decay process of convective turbulence after the maximum eclipse.

The temporal trend for the decay of turbulent kinetic energy is shown in Fig. 8, which occurred in the period

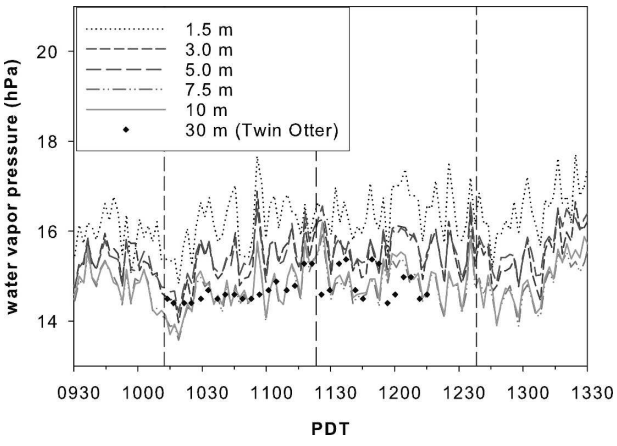

FIG. 6. Same as Fig. 5, but for water vapor pressure.

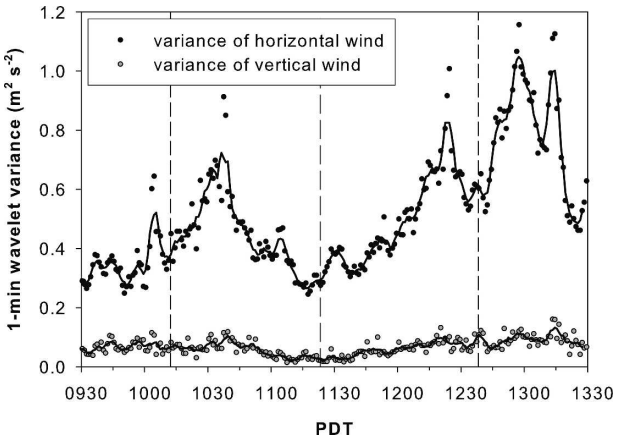

FIG. 7. Wavelet variances of wind components obtained from the wavelet transform of the ASTER sonic data during the eclipse of 11 Jul 1991; solid lines represent the moving average of five consecutive values; dashed vertical lines as in Fig. 4.

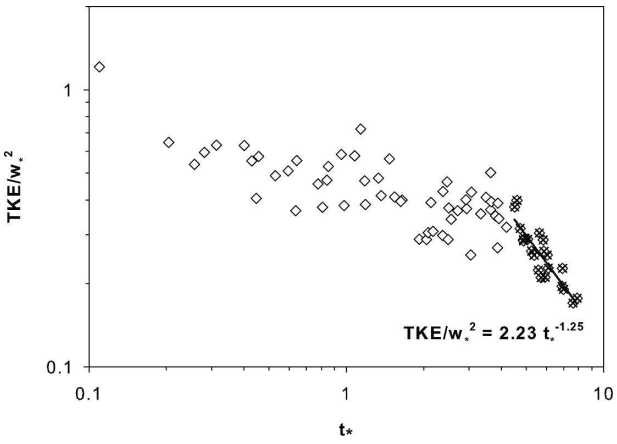

FIG. 8. Temporal trend of the kinetic energy decay obtained from the wavelet transform of the ASTER sonic data from 1124 to 1243 PDT 11 Jul 1991; a power function is fitted to the data measured between 1222 and 1243 PDT, which are overmarked with an "x."

directly after the peak of the eclipse from 1124 to 1238 PDT. Similar to the work of Anfossi et al. (2004), the turbulent kinetic energy (TKE) made dimensionless with the convective velocity scale w_* is presented as a function of the dimensionless time scale $t_* = (t - t_0)z_i/w_*$, with z_i being the boundary layer depth and t_0 the time of the maximum of the eclipse. Those quantities were calculated based on 1-min wavelet variances and covariances. The TKE stayed more or less constant until $t_* = 4.6$, and decayed afterward according to a power law of time with an exponent of -1.25. This exponent is in good agreement with the value of -1.2, which is reported for LES model studies by Nieuwstadt and Brost (1986) and Sorbjan (1997) for a convective boundary layer in which the surface heat flux is set to zero abruptly. However, Anfossi et al. (2004) report an exponent of -2, which is characteristic for a more gradual decrease of the surface heat flux (Sorbjan 1997). The total decay of turbulence occurred not until almost 60 min after the maximum coverage of the eclipse. The power-law part of the decay was between 1222 and 1243 PDT. This coincided with the drop in wind speed variance that we observed at around 1235 PDT. Probably, that drop was a result of the completion of the turbulence decay after the maximum coverage at 1123 PDT. The dimensionless TKE did not start to increase again until 80 min after the maximum coverage.

d. Wavelet cross-scalograms and turbulent fluxes

The wavelet cross-scalograms for the data from the ASTER system are presented in Fig. 9. The cross-scalogram of wT (Fig. 9a) shows that the sensible heat flux was close to zero around 1123 PDT. Afterward, when radiation increased, turbulent transport slowly started in eddies of periods smaller than 100 s. Turbulent transport of sensible heat at longer periods did not reestablish until more than 60 min after the maximum coverage. This is in concurrence with our findings about the turbulent kinetic energy, which did not totally decay until approximately the same time.

An absence of transport at periods longer than 100 s was not observed for water vapor, expressed as absolute humidity ρ_v, and CO_2, expressed as partial density ρ_c. The cross-scalograms for both $w\rho_v$ and $w\rho_c$ show flux contributions at periods of $10^{2.8}$ s (10.5 min) even around 1123 PDT (Figs. 9b,c). Although turbulent transport of these air constituents was significantly reduced during the eclipse (see also Fig. 10), it was not completely shut down. That finding can be explained by the observation that the moisture gradient did not completely disappear during the eclipse (Fig. 6) unlike the air temperature gradient (Fig. 5).

The general patterns in the cross-scalograms of $w\rho_v$ and $w\rho_c$ were very similar. Turbulent transport of water vapor and CO_2 appeared to take place in the same eddies, whereas sensible heat is transported in different ones. Similar structures in the transport of water vapor and CO_2 can, for example, be seen in their cross-scalograms at 1025 PDT and a period of $10^{2.2}$ s, at 1045 PDT and $10^{1.8}$ s, at 1200 PDT and 10^2 s, at 1215 PDT and $10^{1.8}$ s, or at 1250 PDT and 10^2 s. None of these features could be found in cross-scalogram of wT.

The 1-min turbulent fluxes obtained from the wavelet transform of the ASTER tower data agreed in general with the turbulent fluxes measured by the Twin

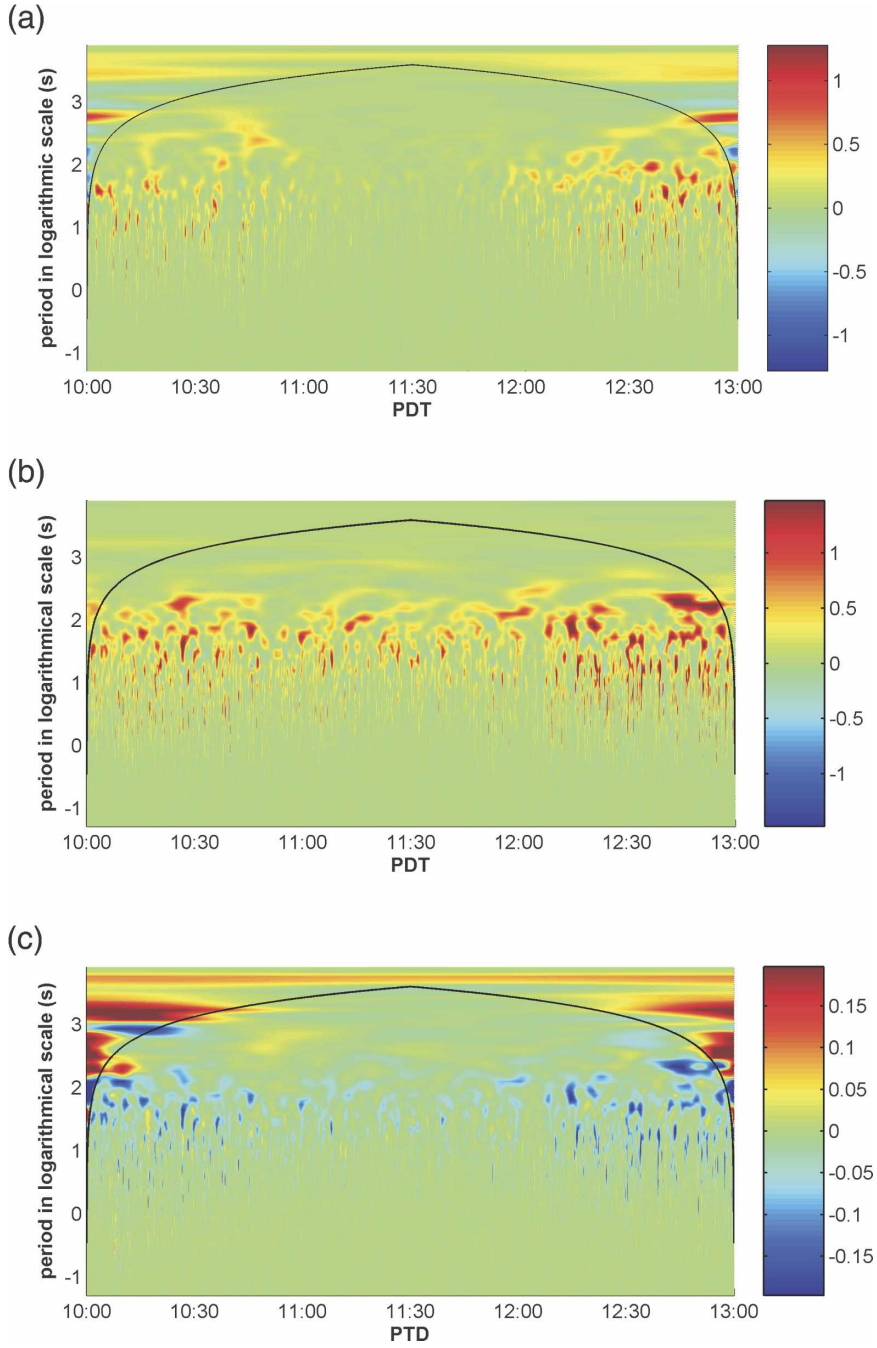

FIG. 9. Morlet wavelet cross-scalograms (area-preserving semilogarithmic presentation) between vertical wind speed w and (a) air temperature T, (b) absolute humidity ρ_v, and (c) carbon dioxide ρ_c, measured at the ASTER tower on the cotton field during the eclipse. The cone of influence from edge effects is indicated by a solid line.

Otter aircraft (Fig. 10). Occasional larger differences, for example, around 1040 PDT for the CO_2 flux, can probably be ascribed to different footprint areas. At that time, an increased sensible heat flux could be observed, which was probably caused by the peak in surface temperature approximately 10 min before. The sensible heat flux had a value over 50 W m^{-2} before the first contact of the eclipse, and becomes almost zero 20 min before maximum coverage. The latent heat flux was significantly reduced to values around 150 W m^{-2} at the time of the maximum coverage relative to values around 250 W m^{-2} before and 500 W m^{-2} after the

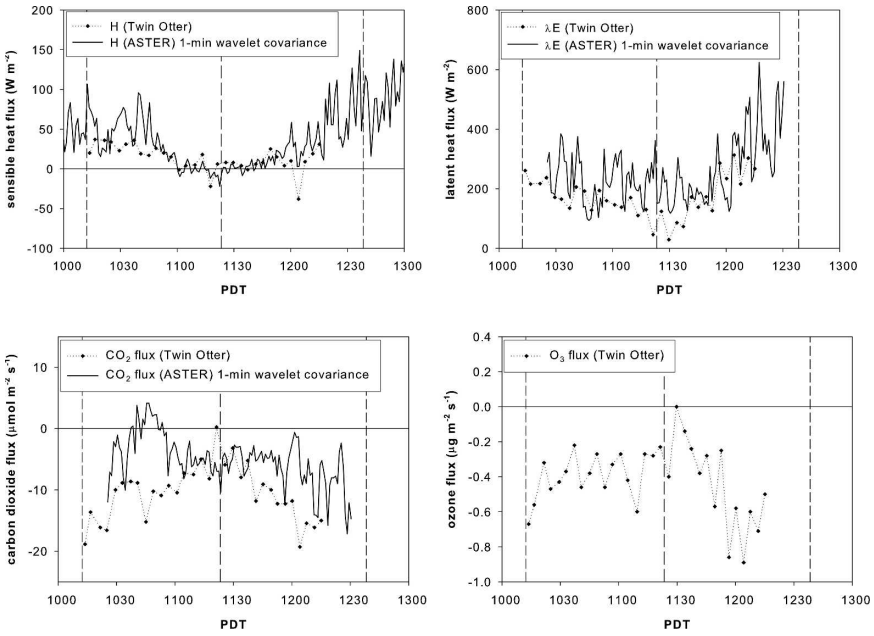

FIG. 10. Turbulent fluxes of (top left) sensible heat H, (top right) latent heat λE, (bottom left) carbon dioxide, and (bottom right) ozone during the eclipse of 11 Jul 1991; dashed vertical lines as in Fig. 4.

eclipse. The latent heat flux was much larger than the sensible heat flux because the whole area was extensively irrigated, assimilation rates of the cotton plants were relatively high, and stomata were wide open.

Turbulent transport of CO_2 was also reduced during the eclipse. Around the maximum coverage the CO_2 flux went down to -3.5 μmol m^{-2} s^{-1} compared to approximately -15 μmol m^{-2} s^{-1} before and after the eclipse. The similar response of the latent heat flux and the CO_2 flux was not unexpected, since the main source or sink of both air constituents is the same, that is, plant stomata. Assimilation and transpiration appeared to be reduced during the eclipse in a similar way. However, they remained active whereas the sensible heat exchange was completely stopped at the time of the maximum coverage.

Unfortunately, the fast-response ozone analyzer of the ASTER system was not operational during the eclipse. The Twin Otter data showed a reduction of the ozone flux from more than -0.5 μg m^{-2} s^{-1} before and after the eclipse to values around -0.2 μg m^{-2} s^{-1} during the maximum coverage. For the interpretation of the O_3 flux, photochemical reactions also have to be considered in addition to turbulent transport, especially during a rapid change in solar radiation. In general during CODE, the atmospheric ozone concentration had a minimum around 0600 PDT and started to increase steadily after sunrise until 1500 PDT (Pederson et al. 1995).

One would expect that the reduction in solar energy due to the eclipse led to a reduced photolytic formation of O_3, and indeed, this can be seen in Fig. 11, where the general trend of increasing O_3 concentrations during a sunny day slowed down and even stopped during the solar eclipse before it increased again after 1150 PDT. A plateau was observed in the otherwise increasing ozone concentrations during the eclipse, in particular for the Twin Otter measurements. The time resolution of the ground-based measurements at the ASTER site was not good enough to show a plateau, but they indicate that the increase of ozone concentrations was reduced during the eclipse. For comparison, ozone concentrations for 21 July 1991 are also shown in Fig. 11 as an example for a similar day without an eclipse.

We found a reduced O_3 deposition (Fig. 10) and a decelerated increase of O_3 concentration (Fig. 11) at the same time. This is in contrast to the observations of Foken et al. (2001) during the total eclipse of 11 August 1999, when both O_3 fluxes and concentrations showed no significant response. These different reactions can possibly be attributed to a different radiation regime there because of the presence of clouds.

All turbulent fluxes show a more or less pronounced minimum (in absolute values) around 1123 PDT. However, these minima may occur with a certain delay after the maximum coverage. This delay, which appears to be different for each turbulent flux, was analyzed by a cross-correlation analysis between the fluxes and the

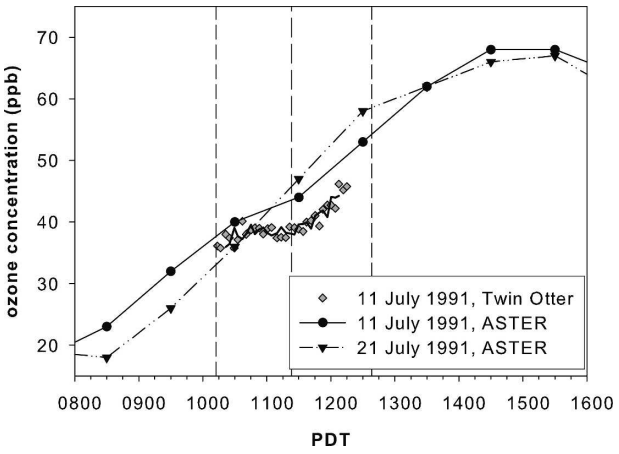

FIG. 11. Ozone concentrations during the solar eclipse measured by the NRC Twin Otter aircraft at an altitude of 30 m above terrain (moving average of five values is given as a black solid line), and ground-based measurements at the ASTER station on the eclipse day and on 21 Jul 1991; dashed vertical lines indicate as in Fig. 4.

solar forcing (Table 1). The only turbulent flux that showed a stronger correlation for a certain delay than for a delay of zero is the sensible heat flux. The delay with the largest correlation coefficient is 13 min for the ASTER dataset and 8 min for the Twin Otter dataset. The delay obtained from the ASTER data is probably more precise since these data have a better temporal resolution.

A statistical test (Papoulis 1990) was performed to determine whether the correlation coefficient with a 13-min delay $r(13\ \text{min})$ is actually significantly different from $r(0\ \text{min})$. According to this test, the probability that the null hypothesis that $r(13\ \text{min}) = r(0\ \text{min})$ is correct is less than 0.279. However, since the Twin Otter data also show a delay, we can probably assume that there is really a delay between the sensible heat flux and the solar forcing, and that it probably ranges between 8 and 13 min.

This delay is almost in agreement with other solar eclipse studies, which investigate delays of the sensible heat flux of 5 min (Foken et al. 2001) or 5–10 min (Eaton et al. 1997). Also, the finding that the turbulent fluxes of CO_2 and O_3 show no significant delay corresponds with Foken et al. (2001). However, our study cannot confirm a delay on the order of 25 min for the latent heat flux, which Foken et al. (2001) report.

5. Summary and conclusions

A wavelet transform was used to characterize the highly nonstationary response of turbulence to a solar eclipse over a cotton field in central California on 11 July 1991. This analysis is now possible thanks to advances in wavelet analysis and in computational capacities during the last decade. The analysis of tower-based measurements complemented with aircraft-based measurements showed significantly reduced turbulence intensity during the eclipse.

TABLE 1. Cross-correlation analysis between incoming shortwave radiation and the turbulent fluxes for the duration of the eclipse (1012–1238 PDT).

ASTER	Correlation coef	Delay (min)	Twin Otter	Correlation coef	Delay (min)
H	0.80	13	H	0.55	8
λE	0.59	0	λE	0.79	<3
CO_2 flux	−0.33	0	CO_2 flux	−0.81	<3
O_3 flux	—	—	O_3 flux	−0.56	<3

Under neutrally stratified conditions in the surface layer, the sensible heat flux went down to zero with a delay to the solar forcing of 8–13 min. After the peak of the eclipse, turbulent transport of sensible heat slowly started in eddies of periods smaller than 100 s before it reestablished completely more than one hour later, after the decay of turbulent kinetic energy had ended following a power law of time with an exponent of −1.25.

Turbulent fluxes of water vapor and CO_2 also showed a strong correlation with the solar radiation. However, these air constituents were transported by different eddies than sensible heat. Both the latent heat flux and the CO_2 flux were significantly reduced by more than 60% during the eclipse but remained active. No time lag could be detected for these two fluxes. The response of the ozone flux also showed no delay to the solar forcing. Ozone deposition was reduced, and the usually positive trend of ozone concentrations before noon was brought to a halt for a time period of 25 min after the maximum coverage.

Acknowledgments. Support for CODE was provided by the San Joaquin Valley Air Pollution Study Agency, the Pacific Gas & Electric Company, and the Electric Power Research Institute. The authors thank the anonymous reviewers for their helpful comments.

REFERENCES

Anderson, J., 1999: Meteorological changes during a solar eclipse. *Weather,* **54,** 207–215.

Anfossi, D., G. Schayes, G. Degrazia, and A. Goulart, 2004: Atmospheric turbulence decay during the solar total eclipse of 11 August 1999. *Bound.-Layer Meteor.,* **111,** 301–311.

Attié, J.-L., and P. Durand, 2003: Conditional wavelet technique applied to aircraft data measured in the thermal internal boundary layer during sea-breeze events. *Bound.-Layer Meteor.,* **106,** 359–382.

Brach, E. J., R. L. Desjardins, and G. St-Amour, 1981: Open path CO_2 analyzer. *J. Phys. E: Sci. Instrum.,* **14,** 1415–1419.

Businger, J. A., W. F. Dabberdt, A. C. Delany, T. W. Horst, C. L. Martin, S. P. Oncley, and S. R. Semmer, 1990: The NCAR Atmospheric-Surface Turbulent Exchange Research (ASTER) facility. *Bull. Amer. Meteor. Soc.,* **71,** 1006–1011.

Chahuneau, F., R. L. Desjardins, E. Brach, and R. Verdon, 1989: A micrometeorological facility for eddy flux measurements of CO_2 and H_2O. *J. Atmos. Oceanic Technol.,* **6,** 193–200.

Cuxart, J., G. Morales, E. Terradellas, and C. Yagüe, 2002: Study of coherent structures and estimation of the pressure transport terms for the nocturnal stable boundary layer. *Bound.-Layer Meteor.,* **105,** 305–328.

Daubechies, I., 1990: The wavelet transform time-frequency localization and signal analysis. *IEEE Trans. Inf. Theory,* **36,** 961–1004.

Desjardins, R. L., J. I. MacPherson, P. H. Schuepp, and F. Karanja, 1989: An evaluation of aircraft flux measurements of CO_2, water vapor and sensible heat. *Bound.-Layer Meteor.,* **47,** 55–69.

——, ——, H. H. Neumann, G. den Hartog, and P. H. Schuepp, 1995: Flux estimates of latent and sensible heat, carbon dioxide and ozone using an aircraft-tower combination. *Atmos. Environ.,* **29,** 3147–3158.

Eaton, F. D., J. R. Hines, W. H. Hatch, R. M. Cionco, J. Byers, D. Garvey, and D. R. Miller, 1997: Solar eclipse effects observed in the planetary boundary layer over a desert. *Bound.-Layer Meteor.,* **83,** 331–346.

Finnigan, J. J., R. Clement, Y. Malhi, R. Leuning, and H. A. Cleugh, 2003: A re-evaluation of long-term flux measurement techniques, Part I: Averaging and coordinate rotation. *Bound.-Layer Meteor.,* **107,** 1–48.

Foken, T., B. Wichura, O. Klemm, J. Gerchau, M. Winterhalter, and T. Weidinger, 2001: Micrometeorological conditions during the total solar eclipse of August 11, 1999. *Meteor. Z.,* **10,** 171–178.

Friehe, C. A., 1991: Air-sea fluxes and surface layer turbulence around a sea surface temperature front. *J. Geophys. Res.,* **96,** 8593–8609.

Goulart, A., G. Degrazia, U. Rizza, and D. Anfossi, 2003: A theoretical model for the study of convective turbulence decay and comparison with large-eddy simulation data. *Bound.-Layer Meteor.,* **107,** 143–155.

Hudgins, L. E., M. E. Mayer, and C. A. Friehe, 1993: Fourier and wavelet analysis of atmospheric turbulence. *Progress in Wavelet Analysis and Applications,* E. Meyers and S. Roques, Eds., Editions Frontiers, 491–498.

Kohsiek, W., 1991: Infrared H_2O/CO_2 sensor with fiber optics. *Proc. Seventh Symp. on Meteorological Observations and Instrumentation,* New Orleans, LA, Amer. Meteor. Soc., 352–355.

Kumar, P., and E. Foufoula-Georgiou, 1994: Wavelet analysis in geophysics: An introduction. *Wavelet in Geophysics,* E. Foufoula-Georgiou and P. Kumar, Eds., Academic Press, 1–43.

MacPherson, J. I., 1990: Wind and flux calculations on the NAE Twin Otter. Institute for Aerospace Research, National Research Council of Canada Rep. LTR-FR-109, 22 pp.

——, 1992: NRC Twin Otter operations in the 1991 California Ozone Deposition Experiment. Institute for Aerospace Research, National Research Council of Canada Rep. LTR-FR-118, 41 pp.

——, R. L. Desjardins, P. H. Schuepp, and R. Pearson, 1995: Aircraft-measured ozone deposition in the San Joaquin Valley of California. *Atmos. Environ.,* **29,** 3133–3145.

Mauder, M., and T. Foken, 2004: Documentation and instruction manual of the eddy covariance software package TK2. Abteilung Mikrometeorologie, Universität Bayreuth Arbeitsergebnisse 26, 44 pp. [Available online at http://www.bitoek.uni-bayreuth.de/mm/.]

Moore, C. J., 1986: Frequency response corrections for eddy correlation systems. *Bound.-Layer Meteor.,* **37,** 17–35.

Nieuwstadt, F. T. M., and R. A. Brost, 1986: The decay of convective turbulence. *J. Atmos. Sci.,* **43,** 532–546.

Oncley, S. P., A. C. Delany, T. W. Horst, and P. P. Tans, 1993: Verification of flux measurement using relaxed eddy accumulation. *Atmos. Environ.,* **27A,** 2417–2426.

——, C. A. Friehe, J. C. Larue, J. A. Businger, E. C. Itsweire, and S. S. Chang, 1996: Surface-layer fluxes, profiles, and turbulence measurements over uniform terrain under near-neutral conditions. *J. Atmos. Sci.,* **53,** 1029–1044.

Papoulis, A., 1990: *Probability and Statistics*. 1st ed. Prentice Hall, 456 pp.

Pederson, J. R., and Coauthors, 1995: California ozone deposition experiment: Methods, results, and opportunities. *Atmos. Environ.,* **29,** 3115–3132.

Schayes, G., J. L. Melice, and V. Dulière, 2002: Surface layer parameters during the solar eclipse of 11 August 1999. *Air Pollution Modeling and Its Applications XV,* C. Borrego and G. Schayes, Eds., Kluwer Academic, 517–518.

Schmidt, R. W. H., A. M. Jochum, and N. Entstrasser, 1991: Airborne ozone flux measurement using a new fast response detector. *Proc. Seventh Symp. on Meteorological Observations and Instrumentation,* New Orleans, LA, Amer. Meteor. Soc., 243–246.

Schotanus, P., F. T. M. Nieuwstadt, and H. A. R. DeBruin, 1983: Temperature measurement with a sonic anemometer and its application to heat and moisture fluctuations. *Bound.-Layer Meteor.,* **26,** 81–93.

Sorbjan, Z., 1997: Decay of convective turbulence revisited. *Bound.-Layer Meteor.,* **82,** 503–517.

Stewart, R. B., and W. R. Rouse, 1974: Radiation and energy budgets at an arctic site during the solar eclipse of July 10, 1972. *Arct. Alp. Res.,* **6,** 231–236.

Strunin, M. A., and T. Hiyama, 2004: Applying wavelet transforms to analyse aircraft-measured turbulence and turbulent fluxes in the atmospheric boundary layer over eastern Siberia. *Hydrol. Processes,* **18,** 3081–3098.

Stull, R. B., 1988: *An Introduction to Boundary Layer Meteorology*. Kluwer Academic, 666 pp.

Swinbank, W. C., 1951: The measurement of vertical transfer of heat and water vapour by eddies in the lower atmosphere. *J. Meteor.,* **8,** 135–145.

Tanner, B. D., E. Swiatek, and J. P. Greene, 1993: Density fluctuations and use of the krypton hygrometer in surface flux measurements. *Management of Irrigation and Drainage Systems: Integrated Perspectives,* R. G. Allen, Ed., American Society of Civil Engineers, 945–952.

Terradellas, E., G. Morales, J. Cuxart, and C. Yagüe, 2001: Wavelet methods: Application to the study of the stable atmospheric boundary layer under non-stationary conditions. *Dyn. Atmos. Oceans,* **34,** 225–244.

——, M. R. Soler, E. Ferreres, and M. Bravo, 2005: Analysis of oscillations in the stable atmospheric boundary layer using wavelet methods. *Bound.-Layer Meteor.,* **114,** 489–518.

Thomas, C., and T. Foken, 2005: Detection of long-term coherent exchange over spruce forest using wavelet analysis. *Theor. Appl. Climatol.,* **80,** 91–104.

Torrence, C., and G. P. Compo, 1998: A practical guide to wavelet analysis. *Bull. Amer. Meteor. Soc.,* **79,** 61–78.

Webb, E. K., G. I. Pearman, and R. Leuning, 1980: Correction of the flux measurements for density effects due to heat and water vapour transfer. *Quart. J. Roy. Meteor. Soc.,* **106,** 85–100.

Wilczak, J. M., S. P. Oncley, and S. A. Stage, 2001: Sonic anemometer tilt correction algorithms. *Bound.-Layer Meteor.,* **99,** 127–150.

Zhang, S. F., J. C. Wyngaard, J. A. Businger, and S. P. Oncley, 1986: Response characteristics of the U.W. sonic anemometer. *J. Atmos. Oceanic Technol.,* **3,** 315–323.